Journal of Medicinal Chemistry

pubs.acs.org/jmc

Article

Novel *N*-Methylated Cyclodepsipeptide Prodrugs for Targeted Cancer Therapy

Chunlei Wu,[#] Zhehong Cheng,[#] Danyi Lu, Ke Liu, Yulian Cheng, Pengxin Wang, Yimin Zhou, Meiqing Li, Ximing Shao, Hongchang Li,* Wu Su,* and Lijing Fang*

Cite This: *J. Med. Chem.* 2021, 64, 991−1000

Read Online

ACCESS | Metrics & More | Article Recommendations | Supporting Information

ABSTRACT: Coibamide A (**1**) is a highly *N*-methylated cyclodepsipeptide with low nanomolar antiproliferative activities against various cancer cell lines. In previous work, we discovered a simplified analogue, [MeAla3-MeAla6]-coibamide (**1a**), which exhibited the same inhibitory abilities as coibamide A. Herein, to reduce the whole-body toxicity and improve the solubility of **1a**, two novel peptide−drug conjugates RGD-SS-CA (**2**) and RGD-VC-CA (**3**) were designed, synthesized, and evaluated. Composed of cyclodepsipeptide **1a**, a tumor-homing RGD motif, and a conditionally labile linker, the conjugates are expected to release **1a** tracelessly in specific tumor microenvironments. Compared with RGD-VC-CA (**3**), RGD-SS-CA (**2**) proved to be superior in in vitro drug release and cytotoxicity tests. Notably, intravenous injection of RGD-SS-CA (**2**) into mice-bearing human tumor xenografts induced significant tumor growth suppression with negligible toxicity. Therefore, as a novel prodrug of the coibamide A analogue, conjugate **2** has great potential for further exploration in cancer drug discovery.

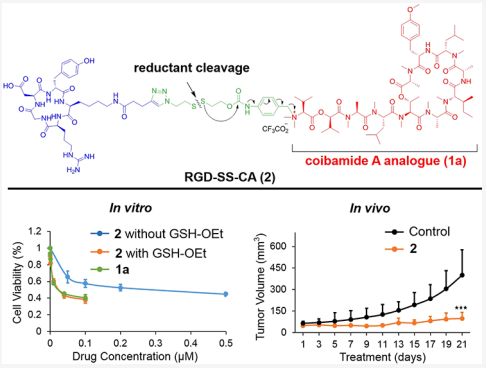

INTRODUCTION

Cyclic peptides discovered from natural sources are a privileged and yet underexploited class of compounds for drug discovery.[1−3] Coibamide A (**1**), isolated from a marine filamentous cyanobacterium by McPhail and co-workers, is a highly *N*-methylated cyclodepsipeptide.[4] Such structural features endow coibamide A with superior pharmacological parameters such as metabolic stability, lipophilicity, and receptor selectivity.[5,6] As a potent cancer cell toxin, coibamide A inhibits the proliferation, migration, and invasion of cancer cells at subnanomolar concentrations.[7] Ishmael et al. have determined that coibamide A induces a rapid and sustained autophagic response via an mTOR-independent mechanism and also induces morphologically and biochemically distinct forms of cell death according to the cell type.[8] Coibamide A directly binds to Sec61α through a distinct binding mode, resulting in a broad substrate-nonselective inhibition of the endoplasmic reticulum (ER) protein import and potent cytotoxicity against specific cancer cell lines.[9] Hence, there has been considerable interest in the use of coibamide A as a promising lead agent in cancer drug discovery.

In previous work, our group accomplished the first total synthesis of coibamide A and revised two stereochemical assignments of the originally proposed structure.[10] Through structure−activity relationship (SAR) studies, we discovered a simplified analogue, [MeAla3-MeAla6]-coibamide A (**1a**) (Figure 1), which not only showed nearly the same antiproliferation activities as coibamide A against the tested cancer cells but also greatly inhibited tumor growth in vivo.[11] As reported by Ishmael et al., coibamide A could cause different patterns of weight loss at the dosage of 0.3 mg/kg through intratumoral injection.[7] However, we did not observe obvious weight losses and side effects in the **1a**-treated group at the same dosage by subcutaneous injection, suggesting that **1a** might have lower toxicity than **1**. In a following study, we found that the intravenous injection of **1a** at the dosage of 1 mg/kg would result in rapid weight loss in the treated mice. In addition, the solubility of **1a** is very poor in a physiological environment. In view of these limitations, we focused our efforts on the development of effective targeted delivery strategies that could be used to temporarily circumvent the bioactivity and enhance the therapeutic efficiency of coibamide A and its analogues.

Stimuli-responsive peptide−drug conjugates (PDCs), called "smart" prodrugs, due to their site-specific and effective drug release characteristics, have been deemed promising agents to indirectly enhance the therapeutic efficiency and reduce the severe side effects of highly toxic agents.[12,13] Compared with antibody−drug conjugates (ADCs), "smart" PDCs can be

Received: August 24, 2020
Published: January 8, 2021

https://dx.doi.org/10.1021/acs.jmedchem.0c01387
J. Med. Chem. 2021, 64, 991−1000

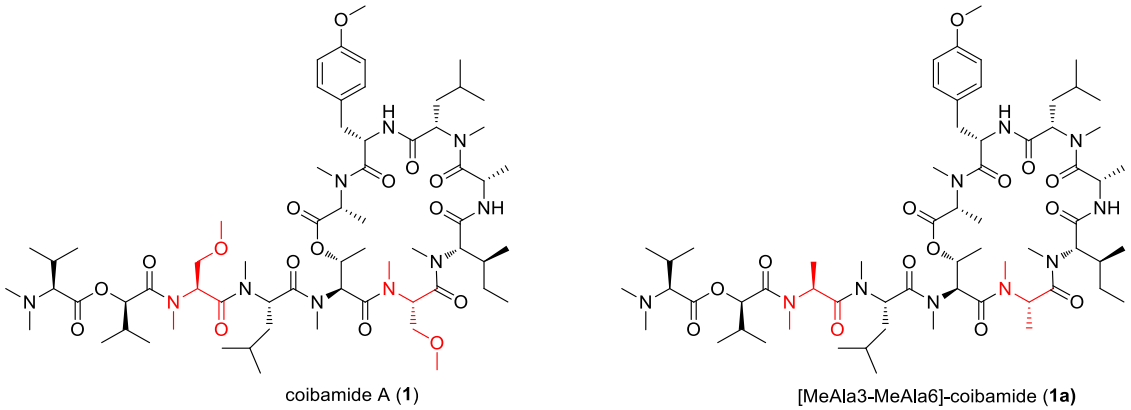

Figure 1. Structures of coibamide A and its simplified analogue [MeAla3-MeAla6]-coibamide (**1a**).

easily prepared by conjugating cytotoxic drugs and specific targeting peptides via conditionally labile linkers, with the advantages of small size, structural homogeneity, and penetration deep into tumors.[14] The utilization of peptides allows the tuning of the physicochemical and biological properties of drugs, in addition to providing targeting ability and improving hydrophilicity.[12] The conditionally labile linkers responsive to pH,[15] redox,[16,17] enzymes,[18,19] and reactive oxygen species (ROS),[20,21] among others, have been developed to temporarily mask the toxicity of drugs and release active molecules under specific tumor microenvironments. In recent years, self-immolating spacers, such as *p*-aminobenzyl derivatives, that can be spontaneously eliminated to yield active molecules using enzyme or glutathione (GSH) have been utilized in drug delivery and fluorescence-based probe design.[22−25] To connect with *p*-aminobenzyl derivatives, functional groups such as amino or hydroxy groups in drugs are commonly required for carbamate or carbonate formation. Although coibamide A and its analogue **1a** have no such functional groups, we noticed that the tertiary amine on their *N*-terminus could be used to connect with *p*-aminobenzyl through quaternary ammonium salt formation. In addition, a charged quaternary ammonium functional group would provide better water solubility, decreased aggregation, and potentially improved therapeutic properties, as discovered by Pillow et al. for the assembly of ADCs with tertiary and heteroaryl amines.[25] Therefore, we anticipated that stimuli-responsive peptide−drug conjugates could be constructed by the reversible attachment of [MeAla3-MeAla6]-coibamide (**1a**) to a targeting peptide in a *p*-aminobenzyl quaternary ammonium salt (PABQ) form.

Integrin $\alpha_v\beta_3$ plays a major role in cell−matrix interactions and in tumorgenesis and is overexpressed in the blood vessels of solid tumors as well as proliferating tumor endothelial cells and various tumor cells.[26,27] A characteristic feature of $\alpha_v\beta_3$ integrin is its high binding affinity for the arginyl-glycyl-aspartic acid (RGD) sequence.[28,29] The RGD peptide motif was designed to be pentacyclic peptides (cyclic RGDyK or RGDfK, and cRGD) with the superiorities of high stability and hydrophilicity. They have been widely applied in targeted cancer imaging and therapy through conjugating with fluorophores, drugs, or nanomaterials.[30−33] Hence, we decided to use the cRGD peptide as the targeting ligand to construct the peptide−drug conjugates of **1a**, thus endowing the conjugates with targeting specificity and improving their water solubility.

In the current work, two novel smart peptide−drug conjugates RGD-SS-CA (**2**) and RGD-VC-CA (**3**) were designed, synthesized, and evaluated. Composed of a tumor-homing peptide with the cRGDyK sequence, cyclodepsipeptide **1a**, and a reduction-cleavable disulfide linker or an enzyme-responsive dipeptide linker, the conjugates are expected to release **1a** tracelessly in specific tumor microenvironments with high levels of GSH and cathepsin B, respectively. Compared with RGD-VC-CA (**3**), RGD-SS-CA (**2**) proved to be superior in in vitro drug release and cytotoxicity tests. Notably, RGD-SS-CA (**2**) significantly suppressed tumor growth in a mouse tumor xenograft model with negligible toxicity and thus has great potential for further exploration in cancer drug discovery.

RESULTS AND DISCUSSION

Design of RGD-CA Conjugates. Two stimuli-responsive RGD-CA conjugates, namely RGD-SS-CA (**2**) and RGD-VC-CA (**3**), were designed by using cRGDyK (cyclic RGD) as a tumor-homing peptide and [MeAla3-MeAla6]-coibamide A (**1a**) as the drug. The structure and release mechanism of conjugates **2** and **3** are shown in Figure 2. For RGD-SS-CA (**2**), cyclic RGD and **1a** were connected through a reduction-cleavable disulfide linker with a *p*-aminobenzyl self-immolative spacer. The cleavage of the disulfide bond by dithiothreitol (DTT) or GSH would induce the intramolecular cyclization to give intermediate **4** with a quaternary ammonium cation in the benzylic position, which underwent 1,6-elimination of the *p*-aminobenzyl group to release the tertiary amine, providing **1a** tracelessly. For RGD-VC-CA (**3**), an enzyme-responsive dipeptide connected to the *p*-aminobenzyl group was used as the linker, in which the valine−citrulline (Val−Cit, VC) dipeptide could be cleaved at the C-terminus of Cit upon exposure to cathepsin B (CTB), a protease upregulated in a variety of cancers, leading to the release of free **1a** through the same benzylic quaternary ammonium intermediate **4**.

Synthesis of Conjugates RGD-SS-CA (2) and RGD-VC-CA (3). The synthetic routes of RGD-SS-CA (**2**) and RGD-VC-CA (**3**) are shown in Scheme 1. Alcohol **5** was obtained from bis(2-hydroxyethyl) disulfide, and dipeptide **9** was prepared through the Fmoc-based solid-phase peptide synthesis. For the synthesis of RGD-SS-CA (**2**), alcohol **5** was reacted with *p*-aminobenzyl alcohol through a BTC-mediated reaction to generate alcohol **6**. Treatment of **6** with thionyl chloride in DCM provided the benzyl chloride intermediate, which was used directly to react with cyclodepsipeptide **1a,**

https://dx.doi.org/10.1021/acs.jmedchem.0c01387
J. Med. Chem. 2021, 64, 991−1000

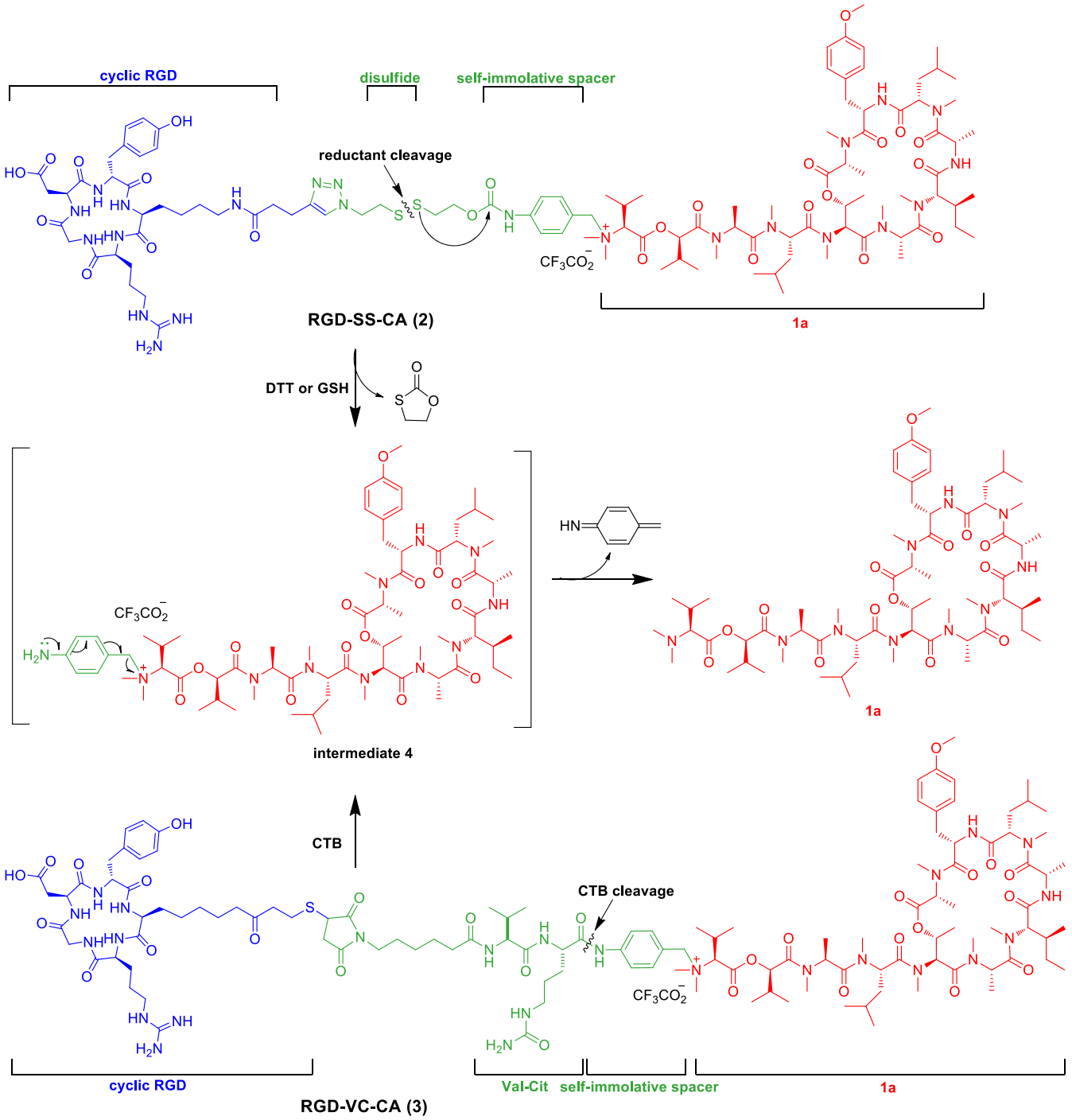

Figure 2. Schematic overview of RGD-SS-CA (**2**) and RGD-VC-CA (**3**) for stimuli-responsive release.

forming quaternary ammonium salt **7**. RGD-SS-CA (**2**) was then obtained by an alkyne−azide cycloaddition reaction of cyclic RGD (**8**) and compound **7**. For the synthesis of RGD-VC-CA (**3**), dipeptide **9** was coupled with *p*-aminobenzyl alcohol in the presence of DIC/HOAT to yield alcohol **10**. Similarly, as described above, chlorination of **10** with thionyl chloride followed by the addition of **1a** generated the quaternary ammonium salt **11**. Finally, RGD-VC-CA (**3**) was prepared by the coupling of **11** bearing a maleimide group and cyclic RGD (**12**) bearing a thiol group under mild conditions. RGD-SS-CA (**2**) and RGD-VC-CA (**3**) were purified using semipreparative RP-HPLC and were validated by HRMS (Figures S5 and S9).

In Vitro Responsive Cleavage of RGD-SS-CA (2) and RGD-VC-CA (3). To demonstrate the stimuli-responsive release of active drug **1a**, the two RGD-CA conjugates were analyzed by RP-HPLC in the presence of DTT and CTB, respectively. First, the stability of conjugates **2** and **3** was studied in PBS at 37 °C. There was no obvious degradation detected under these conditions, with more than 90% of the conjugates remaining intact after 24 h (Figure S10). Next, a solution of conjugate **2** (50 μM) was incubated with DTT (150 μM) in PBS at 37 °C, and the mixture was analyzed at

https://dx.doi.org/10.1021/acs.jmedchem.0c01387
J. Med. Chem. 2021, 64, 991−1000

Scheme 1. Synthesis of RGD-SS-CA (2) and RGD-VC-CA (3)

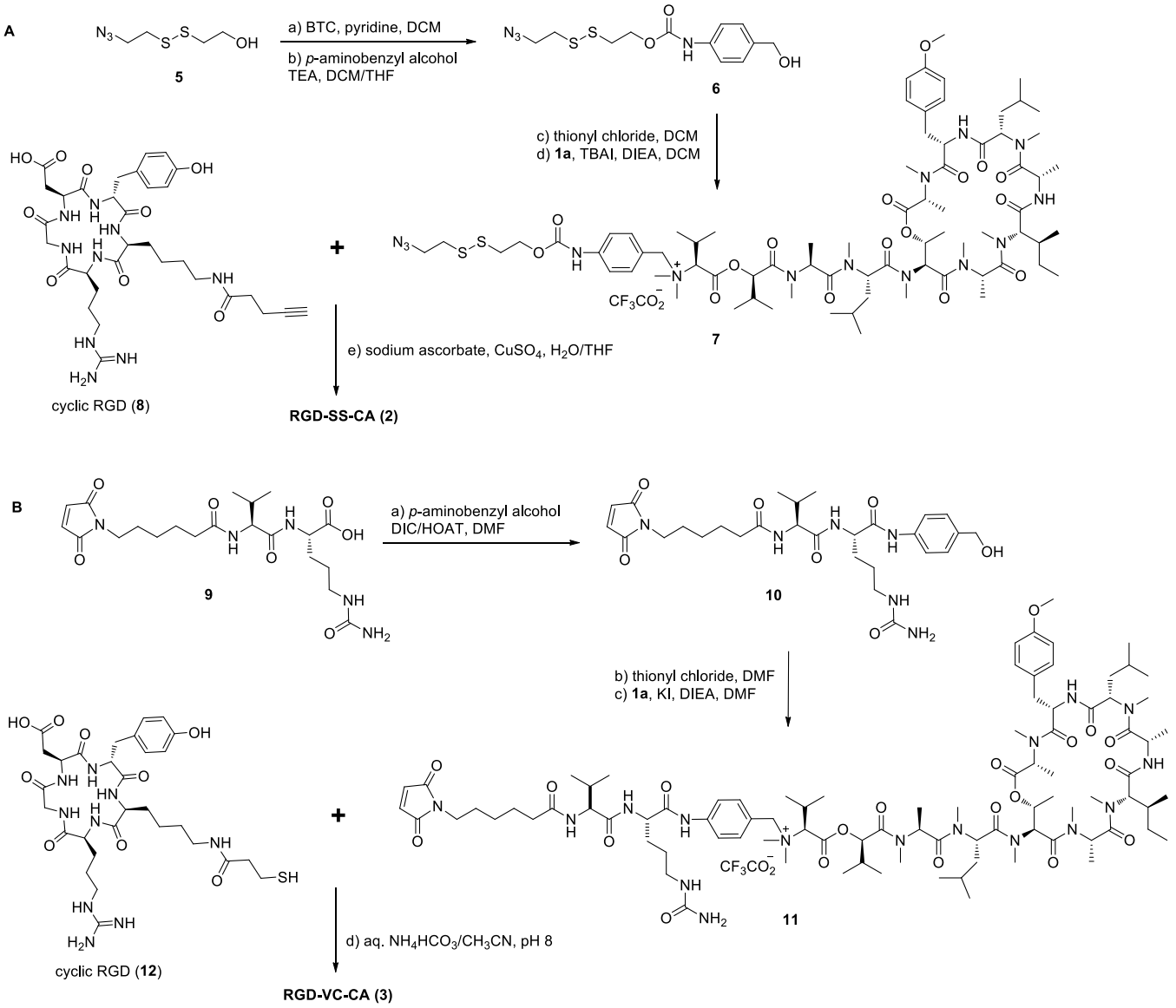

different times. As shown in Figure 3A, after incubation with DTT for 30 min, the peak of **2** (16.07 min) reduced remarkably, while a new strong peak emerged at 18.08 min, which was identified to be **1a**. From 30 to 90 min, a gradual decrease of **2** and an increase of **1a** were observed. At 90 min, the peak of **2** disappeared, indicating that this conjugate was completely cleaved. For RGD-VC-CA (**3**), upon treatment with CTB for 4 h, free **1a** was also discovered at 18.08 min (Figure 3B). However, this cleavage reaction was slow since more than 40% of **3** still existed in the cleavage solution after incubation for 24 h. These results indicated that RGD-SS-CA (**2**) and RGD-VC-CA (**3**) were able to be cleaved to give free **1a** in the presence of DTT and CTB, respectively, but the CTB-responsive release was much slower than the reduction-responsive release.

Cytotoxicity Evaluation. The cytotoxicity of RGD-SS-CA (**2**), RGD-VC-CA (**3**), and **1a** against the human breast cancer cell line BT549 and the human non-small-cell lung cancer cell line A549 was investigated using a standard CCK-8 cell viability assay. Both of the cell lines are integrin $\alpha_v\beta_3$ positive.[34,35] In our previous study, **1a** exhibited high inhibitory activities (in the nanomolar range) against a number of cancer cell lines. The cytotoxicity of **1a** is no different between the two cell lines with the IC_{50} values of 18.0 ± 8.0 nM in BT549 cells and 19.1 ± 8.7 nM in A549 cells after 48 h incubation (Table 1). The cytotoxicity of the three compounds ranked from the greatest to the least: **1a** > **2** > **3**. As shown in Figure 4A and Table 1, for BT549 cells, the IC_{50} values of conjugates **2** (310.7 ± 74.6 nM) and **3** (2.65 ± 0.16 μM) were decreased 16-fold and 146-fold, respectively, in comparison with **1a** (18.0 ± 8.0 nM). For A549 cells, each conjugate displayed similar cytotoxicity profiles to the BT549 cells (Figure 4 and Table 1). Compared with 48 h incubation, the cytotoxicity of **1a**, **2**, and **3** increased in both cell lines after 72 h incubation, but the change trend is similar (Figure S11 and Table S1). In conclusion, the cytotoxicity of **1a** was reduced greatly through the strategy of forming peptide−drug conjugates. Since the cytotoxicity of **3** was much less than **2**, we inferred that the cleavage of a disulfide linker occurred more easily and faster in cancer cells compared with the enzyme-responsive linker, which is consistent with the results of the in vitro-responsive cleavage of the conjugates.

https://dx.doi.org/10.1021/acs.jmedchem.0c01387
J. Med. Chem. 2021, 64, 991−1000

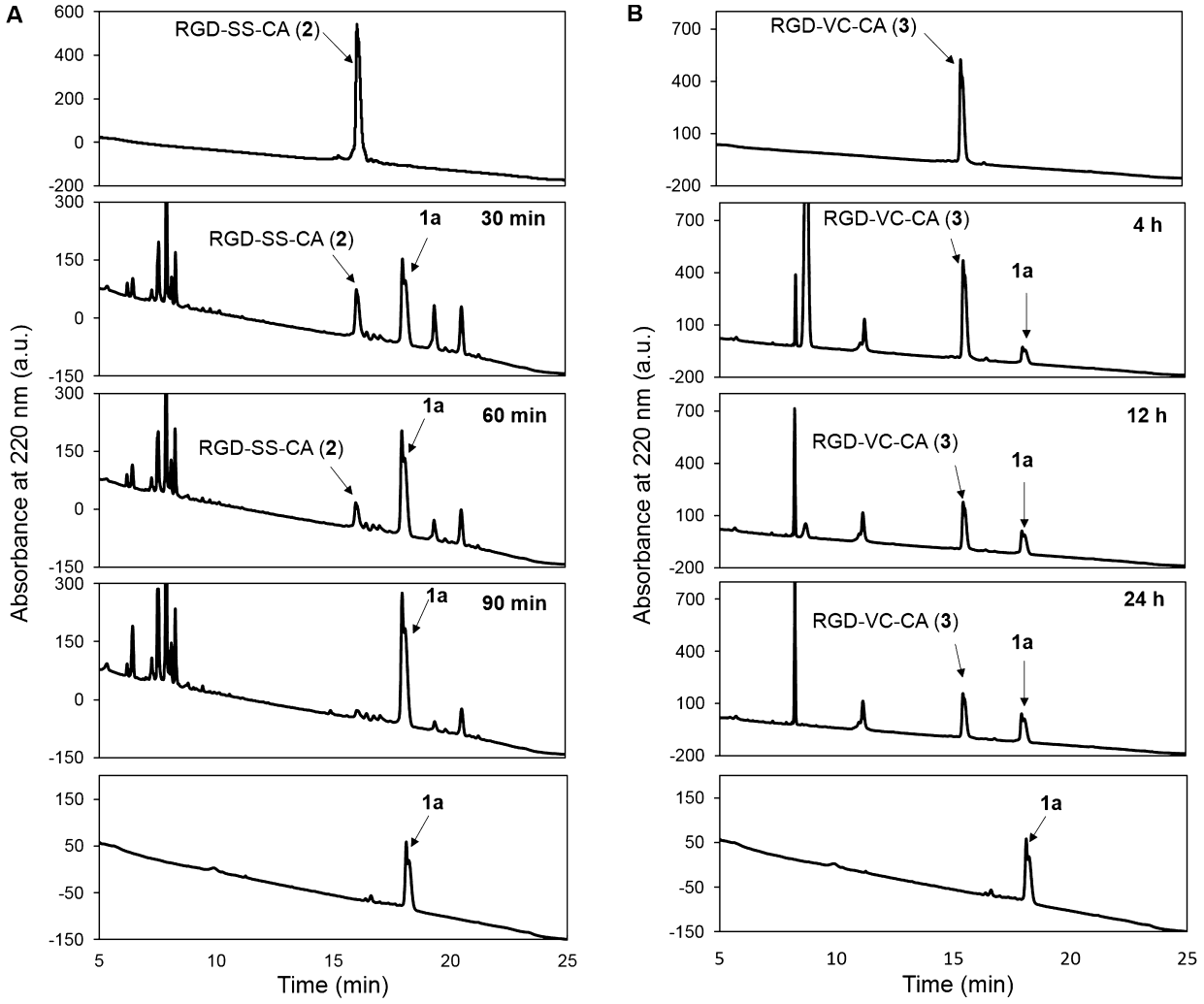

Figure 3. Responsive cleavage of RGD-SS-CA (**2**) and RGD-VC-CA (**3**) in the presence of DTT and CTB, respectively, analyzed by RP-HPLC.

Table 1. IC_{50} Values of RGD-SS-CA (2), RGD-VC-CA (3), and 1a against BT549 and A549 Cells after 48 h of Treatment

compounds	calcd IC_{50} values ± SD (nM)	
	BT549	A549
1a	18.0 ± 8.0	19.1 ± 8.7
RGD-SS-CA (**2**)	310.7 ± 74.6[a]	261.7 ± 95.5[a]
		20.6 ± 7.3[b]
RGD-VC-CA (**3**)	2.65 ± 0.16 (μM)	2.72 ± 0.43 (μM)

[a]Values were measured in the absence of GSH-OEt. [b]Values were measured in the presence of GSH-OEt. IC_{50} values are average of triplicate. SD is the standard deviation of the mean.

Additionally, it is possible that conjugate **3** was located in the cytoplasm after uptake by cells, where the CTB activity is low. In contrast, the high concentration of GSH in cancer cell cytoplasm can explain the higher cytotoxicity of **2**.

Considering that conjugate **2** exhibited preferable cytotoxicity compared to **3**, we selected **2** to conduct the subsequent experiments. The in vitro cytotoxicity of **2** was tested in the presence of GSH-OEt, which can easily penetrate cell membranes and thus increase intracellular GSH concentration through ethyl ester hydrolysis in the cytoplasm.[36] A549 cells were preincubated with GSH-OEt (1 mM) for 2 h, followed by the addition of **2** and coincubation for 48 h. According to the cytotoxicity results (Figure 4C and Table 1), the IC_{50} value of **2** was greatly reduced from 261.7 ± 95.5 nM (without GSH-OEt) to 20.6 ± 7.3 nM, which is almost the same as the IC_{50} value of free **1a** (19.1 ± 8.7 nM). On the other hand, the influence of the cyclic RGD segment, which was generated during the reductive cleavage of conjugate **2**, could be excluded since cyclic RGD (**8**) exhibited no cytotoxicity against both BT549 and A549 cells (Figure 4A,B). Combined, these results indicate that conjugate **2** has nearly the same potency as **1a** under intracellular reductive conditions.

In Vivo Anticancer Activities. We next examined the antitumor activity and the toxicity profile of conjugates **2** and **3** in vivo. Before we studied antitumor activities on tumor-bearing mice, we first compared the solubility of **2** and **3** with **1a**, and discovered that **2** and **3** were about 10-fold more soluble than **1a** in 10% DMSO/PBS. We then evaluated the in vivo toxicity of **1a**, **2**, and **3**. Six-week Balb/c nude male mice (for each group, $n = 3$) were treated with various dosages of **1a** and RGD-CA conjugates by intravenous injection every 2 days. From day 3, we found that 1 mg/kg dosage of **1a** caused rapid weight loss in the treated mice (Figure S12), suggesting that **1a** had high toxicity and was not suitable for in vivo anticancer evaluation. To our delight, no obvious weight losses were observed in the group treated with **2** even at a dosage of 5 mg/

https://dx.doi.org/10.1021/acs.jmedchem.0c01387
J. Med. Chem. 2021, 64, 991−1000

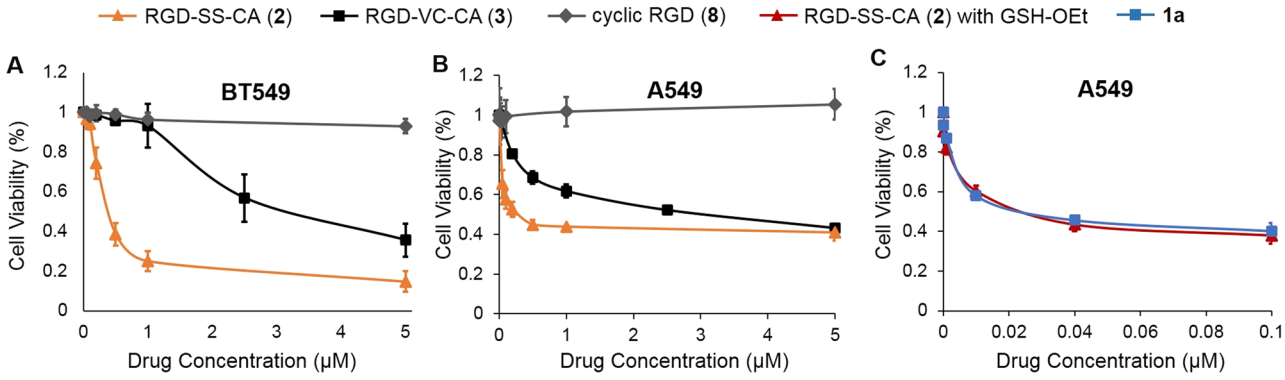

Figure 4. (A, B) Cytotoxicity evaluation of RGD-SS-CA (**2**), RGD-VC-CA (**3**), and cyclic RGD (**8**). (C) Cytotoxicity profiles of RGD-SS-CA (**2**) in the presence of GSH-OEt (1 mM), compared with **1a**. Each experimental point was performed in quadruplicate and each experiment was repeated three times. The cell viability was measured by standard CCK-8 assay after 48 h of treatment.

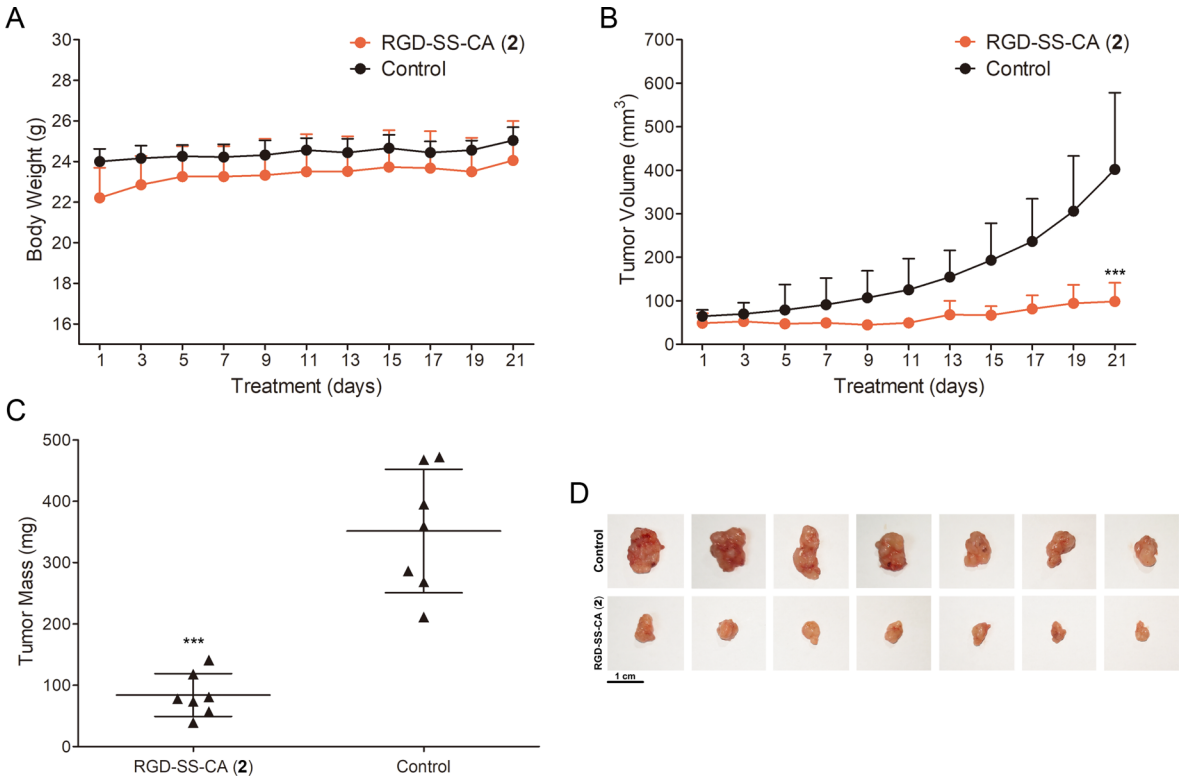

Figure 5. In vivo toxicity and anticancer activity of RGD-SS-CA (**2**) in the mouse tumor xenograft model. In total, 1×10^7 A549 cells were injected subcutaneously into the right flank of each Balb/c nude male mouse, aged 6 weeks. (A) Weight of mice (average ± SD) in the **2**-treated group (male, $n = 7$) and the control group (male, $n = 7$). (B) Tumor volume (average ± SD) of the **2**-treated group and the control group. (C) Tumor mass of the **2**-treated group and the control group. (D) Photograph of the peeled-off tumor of each group. All statistically significant values were calculated by one-way ANOVA. (***): $P < 0.001$. All experiments were performed according to the guideline of the Institutional Ethical Committee of Animal Experimentation of Shenzhen Institute of Advanced Technology, Chinese Academy of Sciences.

kg. Surprisingly, although **3** exhibited less potency in the in vitro cytotoxicity assay, 5 mg/kg of **3** killed all of the mice after two injections, and even 2 mg/kg of **3** could cause severe weight loss. We assume that the release of **1a** from conjugate **3** may intensively occur in the critical organs of the mouse, which can cause severe inflammation or organ failure. Since **2** was about 12-fold less potent than **1a** in the in vitro cytotoxicity assay, a relatively high dosage is needed to reveal the antitumor activities. Moreover, we also want to evaluate the toxicity of **2** at a high dosage in a relatively long term. Therefore, we decided to choose a dosage of 5 mg/kg, equal to 2.7 mg/kg of free **1a**, to proceed with the antitumor evaluation using the A549 tumor xenograft model since the A549 cell line is more sensitive to conjugate **2**. To determine the antitumor activity in vivo, tumor-bearing male mice ($n = 7$) were treated with 5 mg/kg of **2** by intravenous injection every 2 days. As expected, there were no obvious weight losses or other side effects observed over 21 days (Figure 5A). Moreover, the tumor size of the mice treated with **2** remained stable at 50–150 mm^3 without remarkable growth over 3 weeks, whereas the tumors of the vehicle group ($n = 7$) continued to grow at a steady rate. As shown in Figure 5B, the tumor size of the **2**-treated animals was significantly smaller ($P < 0.001$) than that of the vehicle control. At the end of treatment, the mice were

https://dx.doi.org/10.1021/acs.jmedchem.0c01387
J. Med. Chem. 2021, 64, 991−1000

sacrificed, and the tumors were peeled off and weighed. The average tumor mass of the **2**-treated group was nearly 4-fold smaller than that of the vehicle group (Figure 5C,D). These results demonstrated the significant tumor suppression effect of **2** with low side effects in the mouse tumor xenograft model.

CONCLUSIONS

In summary, we have developed two novel peptide−drug conjugates, RGD-SS-CA (**2**) and RGD-VC-CA (**3**), in which the highly *N*-methylated cyclodepsipeptide **1a** was connected with cyclic RGD, a tumor-homing peptide, by a reduction-responsive or an enzyme-responsive linker via the quaternary ammonium salt formation. The incorporation of cyclic RGD and stimuli-responsive linkers not only endows the conjugates with targeting specificity but also improves the solubility of **1a**. Compared with RGD-VC-CA (**3**), RGD-SS-CA (**2**) displayed desirable stimulus-triggered release and higher inhibitory activities in vitro. Notably, the significant tumor suppression effect of RGD-SS-CA (**2**) with negligible toxicity was demonstrated in the mouse tumor xenograft model. Therefore, as a novel prodrug of the coibamide A analogue, conjugate **2** has great potential for further exploration in cancer drug discovery. Moreover, the stimulus-triggered traceless release of cyclodepsipeptide in specific tumor microenvironments provides a new approach for further development of coibamide A and its analogues in targeted cancer therapy.

EXPERIMENTAL SECTION

Materials. Bis(2-hydroxyethyl) disulfide, BTC, *p*-aminobenzyl alcohol, TBAI, DIEA, sodium ascorbate, copper sulfate pentahydrate, DIC, HOAT, HATU, 6-maleimidohexanoic acid, and KI were purchased from Energy Chemical. TEA, pyridine, methanesulfonyl chloride, thionyl chloride, anhydrous DCM, anhydrous DMF, and anhydrous THF were purchased from J&K Scientific. Fmoc-Val-OH, Fmoc-Cit-OH, and 2-CTC resin were purchased from GL Biochem. Cyclic RGD (**8**) and cyclic RGD (**12**) were purchased from Synpeptide Co., Ltd.

Characterization Methods. Analytical RP-HPLC was performed on an Agilent 1260 infinity system equipped with a DAD-UV detector using an Agilent Poroshell 120, EC-C18 column (4.6 mm × 100 mm, 2.7 μm). The RP-HPLC gradient was started at 10% of B (CH_3CN) and then increased to 100% of B over 20 min (A: 0.1% TFA in water) with a flow rate of 0.5 mL/min. The purity of the compounds (>95%) was determined by HPLC. Semipreparative RP-HPLC was performed on the ULTIMAT 3000 instrument (DIONEX). UV absorbance was measured using a photodiode array detector at 220 and 254 nm. The RP-HPLC gradient was started at 10% of B (CH_3CN), and then increased to 100% of B over 30 min (A: 0.1% TFA in water). ^{1}H NMR (^{13}C NMR) spectra were recorded with a Bruker AV400 at 400 (100) MHz. Chemical shifts are referenced to the signals resulting from the residual solvent. High-resolution mass spectra were measured with an ABI Q-star Elite.

Synthesis of Compound (5). Bis(2-hydroxyethyl) disulfide (2.28 g, 15 mmol) and triethylamine (3.06 mL, 22 mmol) were dissolved in 10 mL of anhydrous THF. Methanesulfonyl chloride (1.22 mL, 15.7 mmol) was dissolved in 5 mL of anhydrous THF, and the solution was added dropwise to the above mixture at 0 °C. The mixture was stirred at room temperature for 30 min and concentrated in vacuo to remove the solvent. The residue was suspended in 10 mL of DMF followed by the addition of sodium azide (2.93 g, 45 mmol). The slurry was stirred at 60 °C for 6 h. The reaction mixture was diluted with 80 mL of water and extracted three times with ethyl acetate (3 × 25 mL). The combined organic layer was collected and dried over anhydrous Na_2SO_4. After removal of the solvent under reduced pressure, the crude product was purified by silica gel chromatography (PE/EtOAc = 6:1) to give compound **5** as a colorless oil (1.32 g, 49%). ^{1}H NMR (400 MHz, $CDCl_3$): δ 2.80−2.85 (m, *J* = 4.8 Hz, 4H), 3.08 (s, 1H), 3.55−3.60 (t, *J* = 6.8 Hz, 2H), 3.80−3.85 (t, *J* = 4.5 Hz, 2H) ppm (Figure S1).

Synthesis of Compound (6). To the solution of BTC (196 mg, 0.66 mmol) in anhydrous DCM (2 mL), compound **5** (359 mg, 2 mmol) and pyridine (242 μL, 3 mmol) in anhydrous DCM (2 mL) were added at 0 °C. The resulting mixture was stirred at 0 °C for 30 min. Then, the mixture was concentrated in vacuo and the residue was suspended in 2 mL of anhydrous DCM followed by the addition of a mixture of *p*-aminobenzyl alcohol (368.8 mg, 3 mmol) and TEA (416 μL, 3 mmol) in anhydrous DCM and THF (3 mL, 1:1, v:v). The reaction mixture was stirred at room temperature for 30 min, then was diluted with DCM (20 mL), washed twice with 1 M hydrochloric acid (2 × 10 mL), and finally dried over anhydrous Na_2SO_4. The organic phase was concentrated in vacuo to give the crude product, which was purified by silica gel chromatography (PE:EtOAc = 2:1) to provide compound **6** (225 mg, 34%) as a yellow oil. ^{1}H NMR (400 MHz, $CDCl_3$): δ 2.35 (s, 1H), 2.85−2.89 (t, *J* = 6.8 Hz, 2H), 2.95−3.0 (t, *J* = 4.8 Hz, 2H), 3.57−3.62 (t, *J* = 6.8 Hz, 2H), 4.39−4.61 (t, *J* = 4.8 Hz, 2H), 4.60 (s, 2H), 7.13 (s, 1H), 7.26−7.29 (d, *J* = 8.4 Hz, 2H), 7.34−7.36 (d, *J* = 8.0 Hz, 2H) ppm (Figure S2). ^{13}C NMR (100 MHz, $CDCl_3$): δ 37.6, 37.8, 50.0, 62.7, 64.8, 118.8, 128.3, 136.2, 137.1, 153.0 ppm (Figure S3).

Synthesis of Compound (7). *Step 1.* Compound **6** (108 mg, 0.329 mmol) was dissolved in anhydrous DCM (2 mL) and cooled to 0 °C. Thionyl chloride in DCM (1 mol/L, 362 μL, 0.362 mmol) was added dropwise. Following the addition, the reaction mixture was held at 0 °C for 30 min and then increased to room temperature. After successive stirring for 30 min, the mixture was concentrated under reduced pressure. The residue was dissolved in DCM (10 mL) and washed with saturated $NaHCO_3$ solution. The organic layer was collected and dried over anhydrous Na_2SO_4. After removal of the solvent under reduced pressure, the residue was dissolved in anhydrous DCM (2 mL) and used directly without further purification.

Step 2. To the DCM solution of the product obtained from step 1, **1a** (30 mg, 0.024 mmol) and tetrabutylammonium iodide (60 mg, 0.16 mmol) were added, followed by the addition of DIEA (10 μL, 0.057 mmol). The reaction mixture was stirred at room temperature for 5 h and monitored by RP-HPLC. The mixture was purified by semipreparative RP-HPLC. After lyophilization, compound **7** was obtained as a white powder (15 mg, 39%). HRMS (ESI) *m/z*: calcd. for $C_{75}H_{112}N_{14}O_{16}S_2$ $[M]^+$ 1537.8521, found 1537.8517 (Figure S4).

Synthesis of RGD-SS-CA (2). To a solution of compound **7** (28 mg, 0.018 mmol) in THF (1.5 mL), cyclic RGD (**8**) (15 mg, 0.022 mmol) in water (1.4 mL) was added, followed by the addition of sodium ascorbate (1.76 M in H_2O, 50 μL) and $CuSO_4{\cdot}5H_2O$ (0.26 M in H_2O, 50 μL) successively. The reaction mixture was stirred at room temperature overnight and monitored by RP-HPLC. The mixture was purified by semipreparative RP-HPLC to yield RGD-SS-CA (**2**) (12 mg, 30%). HRMS (ESI) *m/z*: calcd. for $C_{107}H_{167}N_{23}O_{25}S_2$ $[M + H]^{2+}$ 1119.0967, found 1119.09595 (Figure S5).

Synthesis of Compound (9). Commercially available 2-CTC resin (0.5 g, 1 mmol/g, 0.5 mmol) was preswelled for 20 min in DCM in a manual solid-phase peptide synthesis vessel (50 mL). The solution was drained. Anhydrous DMF (6 mL), DIEA (260 μL, 1.5 mmol), and Fmoc-Cit-OH (156 mg, 0.5 mmol) were added to the resin. The mixture was agitated for 2 h before the unreacted resin was capped with acetic acid (200 μL). Then, the solvent was drained, and the resin was washed with DMF (4 × 6 mL). A solution of 20% piperidine in DMF (6 mL) was added to the resin, and the resulting suspension was shaken for 5 min. Then, the solution was removed from the resin. Again, a solution of 20% piperidine in DMF (6 mL) was added to the resin, and the resulting suspension was shaken for another 5 min. The solution was drained, and the resin was washed with DMF (4 × 6 mL) and anhydrous DMF (6 mL). Fmoc-Val-OH (678.8 mg, 2 mmol) and HATU (760.4 mg, 2 mmol) were dissolved in anhydrous DMF (3 mL), and DIEA (1 mL, 6 mmol) was added to the mixture. The solution was stirred for 1 min at room temperature before it was transferred to the deprotected peptidyl resin. The

https://dx.doi.org/10.1021/acs.jmedchem.0c01387
J. Med. Chem. 2021, 64, 991−1000

mixture was agitated for 1 h until a negative Kaiser test was observed. Then, the solvent was drained, and the resin was rinsed with DMF (4 × 6 mL). Followed by the removal of the Fmoc group, 6-maleimidohexanoic acid (422.4 mg, 2 mmol) was coupled to the deprotected peptidyl resin using the same method as that used for Fmoc-Val-OH. Then, the resin was washed with DMF (2 × 6 mL) and DCM (4 × 6 mL). After the removal of the Fmoc group, a solution of TFE and HOAc in DCM (TFE/HOAc/DCM = 1:1:8) was added to the deprotected resin. The resulting mixture was shaken at room temperature for 12 h. Then, the resin was removed by filtration through a disposable propylene filter and washed with DCM (20 mL). The organic solution was concentrated under reduced pressure, and the residue was purified by semipreparative RP-HPLC. After lyophilization, compound **9** was obtained (173 mg, 73%). HRMS (ESI) *m/z*: calcd. for $C_{21}H_{34}N_5O_7$ $[M + H]^+$ 468.2453, found 468.2442; calcd. for $C_{21}H_{33}N_5O_7Na$ $[M + Na]^+$ 490.2272, found 490.2269 (Figure S6).

Synthesis of Compound (10). Compound **9** (100 mg, 0.21 mmol), DIC (30 μL, 0.21 mmol), and HOAT (28.6 mg, 0.21 mmol) were suspended in anhydrous DMF (5 mL). After activation for 1 min, *p*-aminobenzyl alcohol (28.4 mg, 0.23 mmol) was added. The reaction mixture was stirred at room temperature until compound **9** was consumed (2−4 h). The mixture was purified by semipreparative RP-HPLC. After lyophilization, compound **10** was obtained as a yellow powder (82 mg, 68%). HRMS (ESI) *m/z*: calcd. for $C_{28}H_{41}N_6O_7$ $[M + H]^+$ 573.3073, found 573.3044; calcd. for $C_{28}H_{40}N_6O_7Na$ $[M + Na]^+$ 595.2856, found 595.2849 (Figure S7).

Synthesis of Compound (11). *Step 1.* To a solution of compound **10** (42 mg, 0.07 mmol) in anhydrous DMF (0.5 mL) was added dropwise a solution of thionyl chloride in DCM (1 mol/L, 84 μL, 0.084 mmol) at 0 °C. The reaction mixture was held at 0 °C for 30 min and then increased to room temperature. After successive stirring for 30 min, the mixture was concentrated under reduced pressure and purified by silica gel chromatography (DCM/MeOH = 5:1) to afford a yellow solid (18 mg, 44%). The ^1H NMR spectrum was consistent with the literature.[25]

Step 2. **1a** (10 mg, 0.008 mmol) and KI (11.6 mg, 0.07 mmol) were added to an anhydrous DMF (0.5 mL) solution of the product obtained from step 1. The reaction mixture was stirred at 50 °C for 24 h and monitored by RP-HPLC. The mixture was purified by semipreparative RP-HPLC. After lyophilization, compound **11** was obtained as a white powder (6 mg, 42%). HRMS (ESI) *m/z*: calcd. For $C_{91}H_{146}N_{16}O_{20}$ $[M + H]^{2+}$ 891.5444, found 891.5463; calcd. For $C_{91}H_{145}N_{16}O_{20}Na$ $[M + Na]^{2+}$ 902.5354, found 902.5357 (Figure S8).

Synthesis of RGD-VC-CA (3). To a solution of **11** (7 mg, 0.004 mmol) in 30% acetonitrile and aqueous NH_4HCO_3 buffer (20 mM, pH 8, 1 mL), cyclic RGD (**12**) (5.7 mg, 0.008 mmol) was added. After being stirred at 0 °C for 2 h, the reaction mixture was purified by semipreparative RP-HPLC to yield RGD-VC-CA (**3**) (6.9 mg, 68%). HRMS (ESI) *m/z*: calcd. for $C_{121}H_{192}N_{25}O_{29}S_2$ $[M + H]^{2+}$ 1245.19745, found 1245.1964 (Figure S9).

In Vitro Drug Release. RGD-SS-CA (**2**) in DMSO (2 mM, 13 μL) was diluted to 50 μM with 10% DMSO/PBS (0.5 mL). After the addition of DTT (15 mM, 5 μL), the mixture was incubated at 37 °C. At predetermined time points, 30, 60, and 90 min, 50 μL of the release medium was withdrawn and analyzed by RP-HPLC. RGD-VC-CA (**3**) in DMSO (2 mM, 13 μL) was diluted to 50 μM in 10% DMSO/citrate buffer (100 mM, pH 5.5, cysteine 20 mM, 0.5 mL). After the addition of a stock solution of CTB (600 U/mL, 15 μL), the mixture was incubated at 37 °C. At predetermined time points, 4, 12, and 24 h, 50 μL of the release medium was withdrawn and analyzed by RP-HPLC. Solutions of compound **2** or **3** in 10% DMSO/PBS (50 μM, 0.5 mL) without DTT and CTB were incubated at 37 °C for stability studies. At predetermined time points, 0, 4, 8, 12, and 24 h, 50 μL of the solution was withdrawn and analyzed by RP-HPLC. Each experiment was repeated three times.

Cell Line and Culture. The human breast cancer cell line BT549 and the human non-small-cell lung cancer cell line A549 were acquired from the Core Facility of Stem Cell Research, Shanghai Institute of Biological Science, Chinese Academy of Sciences, and were cultured in Dulbecco's modified Eagle's medium (DMEM) with high glucose, 10% fetal bovine serum (Gibco, New Zealand), 100 U/mL penicillin, and 100 μg/mL streptomycin (Hyclone, USA). The cells were incubated in a humidified cell incubator with 5% CO_2 at 37 °C.

Cell Growth Inhibition Assay. In total, 3000−4000 cells were seeded in flat-bottomed 96-well plates and were preincubated overnight. Compounds were diluted in a medium to a gradient of concentration and were used to treat with cells in quadruple for 48 h. The medium was removed carefully, and the cell proliferation reagent CCK-8 (10% in fresh medium, 200 μL) was added to each well and incubated for 1 h at 37 °C. The absorbance at 450 nm was measured by using a Multiskan GO (Thermo Fisher Scientific) and was directly proportional to live cell numbers. Each experiment was repeated three times using four replicates. IC_{50} values were calculated using log(inhibitor) versus response fitting by GraphPad Prism 5.0 and were reported as mean ± SD from three independent experiments.

Animals. Six-week Balb/c nude male mice were purchased from Beijing Vital River Laboratory Animal Technology Co., Ltd. All animal studies complied with the principles of care and use of laboratory animals and were approved by the Institutional Ethical Committee of Animal Experimentation of Shenzhen Institute of Advanced Technology, Chinese Academy of Science.

In Vivo Antitumor Evaluation in a Mouse Tumor Xenograft Model. Six-week Balb/c nude male mice were chosen to establish the tumor xenograft model. After collection by centrifugation and washing twice in cold PBS, 1×10^7 A549 cells were suspended in serum-free DMEM with high glucose and were injected subcutaneously at the right flank of each mouse. After the tumor size reached ∼50 mm^3 ($L \times W \times 1/2\ W$), the animals were randomly divided into two groups (for each group, $n = 7$). A dosage of 5 mg/kg RGS-SS-CA (**2**) in 10% DMSO/PBS (1 mg/mL, 100 μL) was injected intravenously through the tail vein every 2 days for a total of 10 times. Equal volume of 10% DMSO/PBS was used as a vehicle control. Tumor size and mouse weight were measured before each injection. After 10 times of injections, the mice were sacrificed and the tumors were peeled off and weighed.

Statistical Analysis. All data are expressed as the mean ± SD. Statistical analyses were performed using one-way analysis of variance (ANOVA) through GraphPad Prism 5.0 to assess between-group differences. $^*P < 0.05$ was considered statistically significant.

■ ASSOCIATED CONTENT

Supporting Information

The Supporting Information is available free of charge at https://pubs.acs.org/doi/10.1021/acs.jmedchem.0c01387.

NMR and HRMS spectra of the new compounds; RP-HPLC analysis of compounds **2**, **3**, and **1a**; stability studies of **2** and **3**; and the in vivo toxicity of **2** and **1a** (PDF)

Molecular formula strings (XLSX)

■ AUTHOR INFORMATION

Corresponding Authors

Hongchang Li − *Guangdong Key Laboratory of Nanomedicine, Institute of Biomedicine and Biotechnology, Shenzhen Institute of Advanced Technology, Chinese Academy of Sciences, Shenzhen, Guangdong 518055, China*; Phone: (+86)755-86585228; Email: hc.li@siat.ac.cn

Wu Su − *Guangdong Key Laboratory of Nanomedicine, Institute of Biomedicine and Biotechnology, Shenzhen Institute of Advanced Technology, Chinese Academy of Sciences, Shenzhen, Guangdong 518055, China*; orcid.org/0000-0001-9958-3434; Phone: (+86)755-86585203; Email: wu.su@siat.ac.cn

https://dx.doi.org/10.1021/acs.jmedchem.0c01387
J. Med. Chem. 2021, 64, 991−1000

Lijing Fang − *Guangdong Key Laboratory of Nanomedicine, Institute of Biomedicine and Biotechnology, Shenzhen Institute of Advanced Technology, Chinese Academy of Sciences, Shenzhen, Guangdong 518055, China; University of Chinese Academy of Sciences, Beijing 100049, China;* orcid.org/0000-0001-7355-3923; Phone: (+86)755-86392414; Email: lj.fang@siat.ac.cn

Authors

Chunlei Wu − *Guangdong Key Laboratory of Nanomedicine, Institute of Biomedicine and Biotechnology, Shenzhen Institute of Advanced Technology, Chinese Academy of Sciences, Shenzhen, Guangdong 518055, China*

Zhehong Cheng − *Guangdong Key Laboratory of Nanomedicine, Institute of Biomedicine and Biotechnology, Shenzhen Institute of Advanced Technology, Chinese Academy of Sciences, Shenzhen, Guangdong 518055, China*

Danyi Lu − *Guangdong Key Laboratory of Nanomedicine, Institute of Biomedicine and Biotechnology, Shenzhen Institute of Advanced Technology, Chinese Academy of Sciences, Shenzhen, Guangdong 518055, China*

Ke Liu − *Guangdong Key Laboratory of Nanomedicine, Institute of Biomedicine and Biotechnology, Shenzhen Institute of Advanced Technology, Chinese Academy of Sciences, Shenzhen, Guangdong 518055, China*

Yulian Cheng − *Guangdong Key Laboratory of Nanomedicine, Institute of Biomedicine and Biotechnology, Shenzhen Institute of Advanced Technology, Chinese Academy of Sciences, Shenzhen, Guangdong 518055, China*

Pengxin Wang − *Guangdong Key Laboratory of Nanomedicine, Institute of Biomedicine and Biotechnology, Shenzhen Institute of Advanced Technology, Chinese Academy of Sciences, Shenzhen, Guangdong 518055, China; Key Laboratory of Preclinical Study for New Drugs of Gansu Province, School of Basic Medical Sciences, Lanzhou University, Lanzhou, Gansu 730000, China*

Yimin Zhou − *Guangdong Key Laboratory of Nanomedicine, Institute of Biomedicine and Biotechnology, Shenzhen Institute of Advanced Technology, Chinese Academy of Sciences, Shenzhen, Guangdong 518055, China*

Meiqing Li − *Guangdong Key Laboratory of Nanomedicine, Institute of Biomedicine and Biotechnology, Shenzhen Institute of Advanced Technology, Chinese Academy of Sciences, Shenzhen, Guangdong 518055, China; University of Chinese Academy of Sciences, Beijing 100049, China*

Ximing Shao − *Guangdong Key Laboratory of Nanomedicine, Institute of Biomedicine and Biotechnology, Shenzhen Institute of Advanced Technology, Chinese Academy of Sciences, Shenzhen, Guangdong 518055, China*

Complete contact information is available at: https://pubs.acs.org/10.1021/acs.jmedchem.0c01387

Author Contributions

#C.W. and Z.C. contributed equally. The manuscript was written through contributions of all authors. All authors have given approval to the final version of the manuscript.

Notes

The authors declare no competing financial interest.

■ ACKNOWLEDGMENTS

This work was supported by the National Natural Science Foundation of China (Grant Nos. 21672254, 21778068, and 21977111), the Shenzhen Science and Technology Innovation Commission (Grant Nos. JCYJ20170818153538196 and JCYJ20170818162642882), and the Natural Science Foundation of Guangdong Province (Grant Nos. 2019A1515012073 and 2018B030308001). The authors appreciate the Peking University Shenzhen Graduate School for the assistance of Mass facility.

■ ABBREVIATIONS

BTC, bis(trichloromethyl)carbonate; CH_3CN, acetonitrile; DTT, dithiothreitol; DCM, dichloromethane; DIC, *N,N′*-diisopropylcarbodiimide; DIEA, *N,N′*-diisopropylethylamine; DMF, *N,N′*-dimethylformamide; GSH, glutathione; CTB, cathepsin B; EtOAc, ethyl acetate; HOAc, acetic acid; HOAt, 1-hydroxy-7-aza-benzotriazole; HATU, 2-(7-azabenzotriazol-1-yl)-*N,N,N′,N′*-tetramethyluronium hexafluoro-phosphate; MeOH, methyl alcohol; PE, petroleum ether; TBAI, tetrabutylammonium iodide; TFA, trifluoroacetic acid; TFE, 2,2,2-trifluorethanol; TEA, triethylamine; THF, tetrahydrofuran

■ REFERENCES

(1) Vinogradov, A. A.; Yin, Y.; Suga, H. Macrocyclic peptides as drug candidates: Recent progress and remaining challenges. *J. Am. Chem. Soc.* **2019**, *141*, 4167−4181.

(2) Agrawal, S.; Acharya, D.; Adholeya, A.; Barrow, C. J.; Deshmukh, S. K. Nonribosomal peptides from marine microbes and their antimicrobial and anticancer potential. *Front. Pharmacol.* **2017**, *8*, 828.

(3) Süssmuth, R. D.; Mainz, A. Nonribosomal peptide synthesis-principles and prospects. *Angew. Chem., Int. Ed.* **2017**, *56*, 3770−3821.

(4) Medina, R. A.; Goeger, D. E.; Hills, P.; Mooberry, S. L.; Huang, N.; Romero, L. I.; Ortega-Barria, E.; Gerwick, W. H.; McPhail, K. L. Coibamide A, a potent antiproliferative cyclic depsipeptide from the panamanian marine cyanobacterium Leptolyngbya sp. *J. Am. Chem. Soc.* **2008**, *130*, 6324−6325.

(5) Chatterjee, J.; Laufer, B.; Kessler, H. Synthesis of N-methylated cyclic peptides. *Nat. Protoc.* **2012**, *7*, 432−444.

(6) Morishita, M.; Peppas, N. A. Is the oral route possible for peptide and protein drug delivery. *Drug Discovery Today* **2006**, *11*, 905−910.

(7) Serrill, J. D.; Wan, X.; Hau, A. M.; Jang, H. S.; Coleman, D. J.; Indra, A. K.; Alani, A. W. G.; McPhail, K. L.; Ishmael, J. E. Coibamide A, a natural lariat depsipeptide, inhibits VEGFA/VEGFR2 expression and suppresses tumor growth in glioblastoma xenografts. *Invest. New Drugs* **2016**, *34*, 24−40.

(8) Hau, A. M.; Greenwood, J. A.; Loehr, C. V.; Serrill, J. D.; Proteau, P. J.; Ganley, I. G.; McPhail, K. L.; Ishmael, J. E. Coibamide A induces mTOR-independent autophagy and cell death in human glioblastoma cells. *PLoS One* **2013**, *8*, No. e65250.

(9) Tranter, D.; Paatero, A. O.; Kawaguchi, S.; Kazemi, S.; Serrill, J. D.; Kellosalo, J.; Vogel, W. K.; Richter, U.; Mattos, D. R.; Wan, X.; Thornburg, C. C.; Oishi, S.; McPhail, K. L.; Ishmael, J. E.; Paavilainen, V. O. Coibamide A targets Sec61 to prevent biogenesis of secretory and membrane proteins. *ACS Chem. Biol.* **2020**, *15*, 2125−2136.

(10) Yao, G.; Pan, Z.; Wu, C.; Wang, W.; Fang, L.; Su, W. Efficient synthesis and stereochemical revision of coibamide A. *J. Am. Chem. Soc.* **2015**, *137*, 13488−13491.

(11) Yao, G.; Wang, W.; Ao, L.; Cheng, Z.; Wu, C.; Pang, Z.; Liu, K.; Li, H.; Su, W.; Fang, L. Improved total synthesis and biological evaluation of coibamide A analogues. *J. Med. Chem.* **2018**, *61*, 8908−8916.

(12) Ma, L.; Wang, C.; He, Z.; Cheng, B.; Zheng, L.; Huang, K. Peptide-drug conjugate: A novel drug design approach. *Curr. Med. Chem.* **2017**, *24*, 3373−3396.

(13) Wang, Y.; Cheetham, A. G.; Angacian, G.; Su, H.; Xie, L.; Cui, H. Peptide-drug conjugates as effective prodrug strategies for targeted delivery. *Adv. Drug Deliv. Rev.* **2017**, *110-111*, 112−126.
(14) Fosgerau, K.; Hoffmann, T. Peptide therapeutics: Current status and future directions. *Drug Discovery Today* **2015**, *20*, 122−128.
(15) Sheng, Y.; Xu, J.; You, Y.; Xu, F.; Chen, Y. Acid-sensitive peptide-conjugated doxorubicin mediates the lysosomal pathway of apoptosis and reverses drug resistance in breast cancer. *Mol. Pharmaceutics* **2015**, *12*, 2217−2228.
(16) Ye, M.; Wang, X.; Tang, J.; Guo, Z.; Shen, Y.; Tian, H.; Zhu, W.-H. Dual-channel NIR activatable theranostic prodrug for in vivo spatiotemporal tracking thiol-triggered chemotherapy. *Chem. Sci.* **2016**, *7*, 4958−4965.
(17) Han, H.; Jin, Q.; Wang, Y.; Chen, Y.; Ji, J. The rational design of a gemcitabine prodrug with AIE-based intracellular light-up characteristics for selective suppression of pancreatic cancer cells. *Chem. Commun.* **2015**, *51*, 17435−17438.
(18) Yuan, Y.; Kwok, R. T. K.; Tang, B. Z.; Liu, B. Targeted theranostic platinum(IV) prodrug with a built-in aggregation-induced emission light-up apoptosis sensor for noninvasive early evaluation of its therapeutic responses in situ. *J. Am. Chem. Soc.* **2014**, *136*, 2546−2554.
(19) Cartwright, O. C.; Beekman, A. M.; Cominetti, M. M. D.; Russell, D. A.; Searcey, M. A peptide-duocarmycin conjugate targeting the thomsen-friedenreich antigen has potent and selective antitumor activity. *Bioconjugate Chem.* **2020**, *31*, 1745−1749.
(20) Tao, W.; He, Z. ROS-responsive drug delivery systems for biomedical applications. *Asian J. Pharm. Sci.* **2018**, *13*, 101−112.
(21) Sharma, A.; Lee, M.-G.; Won, M.; Koo, S.; Arambula, J. F.; Sessler, J. L.; Chi, S.-G.; Kim, J. S. Targeting heterogeneous tumors using a multifunctional molecular prodrug. *J. Am. Chem. Soc.* **2019**, *141*, 15611−15618.
(22) Hettiarachchi, S. U.; Prasai, B.; McCarley, R. L. Detection and cellular imaging of human cancer enzyme using a turn-on, wavelength-shiftable, self-immolative profluorophore. *J. Am. Chem. Soc.* **2014**, *136*, 7575−7578.
(23) Liu, G.; Wang, X.; Hu, J.; Zhang, G.; Liu, S. Self-immolative polymersomes for high-efficiency triggered release and programmed enzymatic reactions. *J. Am. Chem. Soc.* **2014**, *136*, 7492−7497.
(24) Yang, Y.; Zhou, T.; Jin, M.; Zhou, K.; Liu, D.; Li, X.; Huo, F.; Li, W.; Yin, C. Thiol-chromene "click" reaction triggered self-immolative for NIR visualization of thiol flux in physiology and pathology of living cells and mice. *J. Am. Chem. Soc.* **2020**, *142*, 1614−1620.
(25) Staben, L. R.; Koenig, S. G.; Lehar, S.; Vandlen, R.; Zhang, D.; Chuh, J.; Yu, S.-F.; Ng, C.; Guo, J.; Liu, Y.; Fourie-O'Donohue, A.; Go, M.; Xin, L.; Segraves, N. L.; Wang, T.; Chen, J.; Wei, B.; Phillips, G. D. L.; Xu, K.; Kozak, K. R.; Mariathasan, S.; Flygare, J. A.; Pillow, T. H. Targeted drug delivery through the traceless release of tertiary and heteroaryl amines from antibody-drug conjugates. *Nat. Chem.* **2016**, *8*, 1112−1119.
(26) Strömblad, S.; Cheresh, D. A. Integrins, angiogenesis and vascular cell survival. *Chem. Biol.* **1996**, *3*, 881−885.
(27) Seguin, L.; Desgrosellier, J. S.; Weis, S. M.; Cheresh, D. A. Integrins and cancer: regulators of cancer stemness, metastasis, and drug resistance. *Trends Cell Biol.* **2015**, *25*, 234−240.
(28) Dijkgraaf, I.; Beer, A. J.; Wester, H. Application of RGD-containing peptides as imaging probes for alphavbeta3 expression. *Front. Biosci.* **2009**, *Volume*, 887−899.
(29) Gamble, L. J.; Borovjagin, A. V.; Matthews, Q. L. Role of RGD-containing ligands in targeting cellular integrins: Applications for ovarian cancer virotherapy. *Exp. Ther. Med.* **2010**, *1*, 233−240.
(30) Qiu, M.; Wang, X.; Sun, H.; Zhang, J.; Deng, C.; Zhong, Z. Cyclic RGD-peptide-functionalized polylipopeptide micelles for enhanced loading and targeted delivery of monomethyl auristatin E. *Mol. Pharmaceutics* **2018**, *15*, 4854−4861.
(31) Araste, F.; Abnous, K.; Hashemi, M.; Taghdisi, S. M.; Ramezani, M.; Alibolandi, M. Peptide-based targeted therapeutics: Focus on cancer treatment. *J. Controlled Release* **2018**, *292*, 141−162.
(32) Ma, X.; Jia, J.; Cao, R.; Wang, X.; Fei, H. Histidine-iridium(III) coordination-based peptide luminogenic cyclization and cyclo-RGD peptides for cancer-cell targeting. *J. Am. Chem. Soc.* **2014**, *136*, 17734−17737.
(33) Han, H.; Valdepérez, D.; Jin, Q.; Yang, B.; Li, Z.; Wu, Y.; Pelaz, B.; Parak, W. J.; Ji, J. Dual enzymatic reaction-assisted gemcitabine delivery systems for programmed pancreatic cancer therapy. *ACS Nano* **2017**, *11*, 1281−1291.
(34) Hill, B. S.; Sarnella, A.; Capasso, D.; Comegna, D.; Gatto, A. D.; Gramanzini, M.; Albanese, S.; Saviano, M.; Zaccaro, L.; Zannetti, A. Therapeutic potential of a novel $\alpha_v\beta_3$ antagonist to hamper the aggressiveness of mesenchymal triple negative breast cancer sub-type. *Cancers* **2019**, *11*, 139.
(35) Pirooznia, N.; Abdi, K.; Beiki, D.; Emami, F.; Arab, S. S.; Sabzevari, O.; Soltani-Gooshkhaneh, S. ^{177}Lu-labeled cyclic RGD peptide as an imaging and targeted radionuclide therapeutic agent in non-small cell lung cancer: Biological evaluation and preclinical study. *Bioorg. Chem.* **2020**, *102*, 104100.
(36) Koo, A. N.; Lee, H. J.; Kim, S. E.; Chang, J. H.; Park, C.; Kim, C.; Park, J. H.; Lee, S. C. Disulfide-cross-linked PEG-poly(amino acid)s copolymer micelles for glutathione-mediated intracellular drug delivery. *Chem. Commun.* **2008**, 6570−6572.

https://dx.doi.org/10.1021/acs.jmedchem.0c01387
J. Med. Chem. 2021, 64, 991−1000